Physica B 462 (2015) 86–92

Contents lists available at ScienceDirect

Physica B

journal homepage: www.elsevier.com/locate/physb

Comprehensive modelling of dynamic hysteresis loops in the rolling and transverse directions for transformer laminations

A.P.S. Baghel [a,*], A. Gupta [a], K. Chwastek [b], S.V. Kulkarni [a]

[a] Department of Electrical Engineering, Indian Institute of Technology Bombay, Mumbai 400076, India
[b] Department of Electrical Engineering Czestochowa University of Technology, Poland

ARTICLE INFO

Article history:
Received 13 October 2014
Received in revised form
27 December 2014
Accepted 22 January 2015
Available online 23 January 2015

Keywords:
Dynamic losses
Magnetic viscosity approach
Grain-oriented laminations
Jiles-atherton model

ABSTRACT

Magnetic properties of grain-oriented materials are affected by hysteresis, anisotropy and dynamic effects. The attempts to describe dynamic hysteresis loops are usually limited to the rolling direction (RD). On the other hand, modelling of magnetic properties for the transverse direction (TD) is important for numerical analysis of core-joints and corner regions in transformers. For this direction, hysteresis loops reveal complex shapes particularly for dynamic magnetization conditions. This paper presents a comprehensive approach for modelling of dynamic hysteresis loops in RD and TD. This work uses the magnetic viscosity-based approach, which is able to describe irregular widening of dynamic loops. The loss separation scheme is also considered for both principal directions. Variations of loss components with frequency for both directions are discussed. The computed dynamic loops in RD and TD are in a close agreement with experimental ones.

1. Introduction

The magnetic properties of grain-oriented (GO) materials used in transformer laminations are affected by a number of phenomena, such as hysteresis, anisotropy, and eddy currents. The mechanisms underlying the physics of magnetization process are well described in the literature [1–4], yet the macroscopic behaviour of the material is still difficult to model. On the other hand, the development of an accurate model for predicting the gross behaviour of these materials is an important issue for the engineering community in order to design efficient electromagnetic devices [5–7]. Favourable crystallographic properties in the rolling direction (RD) of these materials make them ideal for power transformers and large rotating electrical machines. The properties along the directions other than RD are needed for more realistic field computation at joints/teeth regions [8]. For such an analysis, a precise vector hysteresis model is needed [7].

A number of significant attempts have been reported in the literature to characterize the hysteresis loops for the rolling and transverse (TD) directions [9–11]. One possible approach, based on some concepts from chemical/thermo-dynamical theories [9], has been presented in [10]. The latter paper has proven its usefulness for the description of quasi-static RD and TD magnetization curves. Another promising description which is based on the Jiles–Atherton (JA) approach, proposed recently in [11], has also been used for hysteresis loops in two principal directions. This model can also be used further for modelling of hysteresis loops in arbitrary directions, similarly to the description considered in [12], which uses the correlations of intrinsic RD and TD properties. The JA model can be a suitable candidate for hysteresis modelling due to its relative simplicity and ease in numerical implementation [13]. The original JA model is based on some physical premises concerning irreversible domain wall translation through pinning sites in isotropic materials [2]. Hence most of the existing dynamic JA models are focused on these materials [14–17]. Moreover, such model extensions are commonly based on Bertotti's approach [1], which under certain circumstances may fail to predict arbitrary loop shapes and loss vs. frequency dependencies [18,19]. In GO steels, the dynamic effects related to the existence of classical and excess field strengths [1] may be significant, which makes the analysis more difficult. The dynamic hysteresis loops of these materials may exhibit anomalous shapes [19]. The problem of modelling of dynamic hysteresis in TD is rarely addressed in the literature; this paper is aimed to fill the gap.

This paper presents a modelling approach for dynamic hysteresis loops in RD and TD using a viscosity-based extension of the modified quasi-static JA model which considers the crystallographic features of GO materials in order to predict accurately RD and TD static hysteresis loops [11]. The paper also elaborates loss separation using a three-component approach. A generalized approach based on the magnetic viscosity is used for modeling of excess losses in RD and TD. The approach offers flexibility to

* Corresponding author.
E-mail address: ajaybaghel@iitb.ac.in (A.P.S. Baghel).

http://dx.doi.org/10.1016/j.physb.2015.01.026
0921-4526/

handle an arbitrary loss versus frequency dependence and to control anomalous loop shapes in both principal directions [20,21]. A magnetic viscosity based modified dynamic JA model has been proposed recently in [21]. Encouraging modelling results have been obtained for RD dynamic loops.

In the present paper, a comprehensive modeling approach for dynamic loops in RD and TD is described using the model. The approach is consistent with the classical theory of loss separation as the value of classical eddy current loss is kept constant disregarding the applied field direction. The hysteresis and excess losses vary with direction, and these loss components can be computed using the modified quasi-static JA model and the magnetic viscosity based approach, respectively. The arbitrary frequency-loss dependence and anomalies in loop shapes are attributed to the excess loss, which can be handled using the viscous approach.

2. Magnetic properties in the rolling and transverse directions

2.1. Measurement of dynamic hysteresis loops and losses

Measurements are carried out on two samples (Hi–B material; grade – 27M-OH) which are cut at angles of 0° and 90° with respect to RD. The thickness of samples is 0.27 mm, the length is 200 mm, and the width is 29.5 mm. The measurements are performed using a standard single sheet tester (Model: BROCKHAUS MPG 200D). Measurements of hysteresis loops and losses are carried out over a frequency range of 1–200 Hz. It is assumed that the effects of classical eddy currents and excess losses on the hysteresis loop can be neglected at 1 Hz. Hence the obtained hysteresis loops and losses at 1 Hz in are assumed to be static quantities. The peak flux densities are set to 1.7 T and 1.3 T for RD and TD, respectively. Measured hysteresis loops of the material for RD and TD at different frequencies are shown in Fig. 1(a) and (b). A lower value is chosen for TD since the curve saturates earlier in this direction as observed in Fig. 1(b).

As evident from the figures, GO steels show highly steep, gooseneck, and narrow waist hysteresis loops in RD and complex shaped curves in TD. Moreover, an irregular widening (as shown by line-L in the figures) in dynamic loops can also be observed for both directions in these materials. The irregular widening of dynamic loops can be attributed to the excess losses.

2.2. Corelosses

The separation of total core loss into three components viz., hysteretic, classic, and excess terms is a common practice for loss description in thin ferromagnetic laminations [22,23]. The total energy losses can be represented as the sum of the static hysteresis loss, the classical loss, and the excess loss using a thin sheet model (TSM). The loss equation for GO laminations can be written as [23]

$$W_{\text{tot}} = W_{\text{hyst}} + W_{\text{class}} + W_{\text{exc}}, \tag{1}$$

where W_{tot} is the total energy loss, W_{hyst} is the static hysteresis loss, and W_{class} and W_{exc} are the classical and excess losses, respectively. The hysteresis loss, W_{hyst}, was measured in a quasi-static field condition at 1 Hz as the dynamic effects are negligible at this frequency. The classical losses can be calculated using the following equation [1]:

$$W_{class} = k_e \int \left(\frac{dB}{dt}\right) dB \quad \text{where } k_e = \frac{d^2}{12\rho}. \tag{2}$$

Here d and ρ are the sheet thickness and resistivity. The classical losses can be calculated using Eq. (2). The parameter k_e (0.013 (m/Ω)) can also be calculated directly and it remains fixed in different directions (RD and TD) at all frequencies since it depends solely on thickness (d=0.27 mm) and resistivity ($\rho = 4.6 \times 10^{-7}$ Ω m) of the material. The excess energy loss, W_{exc}, is computed as the difference between W_{tot} and the sum of W_{hyst} and W_{class}. These loss components are given in Table 1 for RD and TD for maximum induction of 1.1 T at 50 Hz.

The classical losses are calculated using Eq. (2) derived under the assumption of homogeneous material (devoid of domain structure) and hence it may be assumed that these losses do not vary with the direction of applied field [3]. Only two loss components (hysteresis and excess loss) will change with the direction. The difference in static hysteresis losses in two directions can be explained in terms of the different proportion of 180° and 90° domain walls in TD [3,12]. On the contrary, the excess losses depend on domain wall spacing and types of domain walls (90° and 180° walls) [3,24]. The domain wall spacing varies with crystalline orientation, and hence this anisotropy of the excess loss is not directly related to magnetocrystalline anisotropy [25]. Higher excess losses in TD can also be attributed to 90° wall processes and nucleation [26].

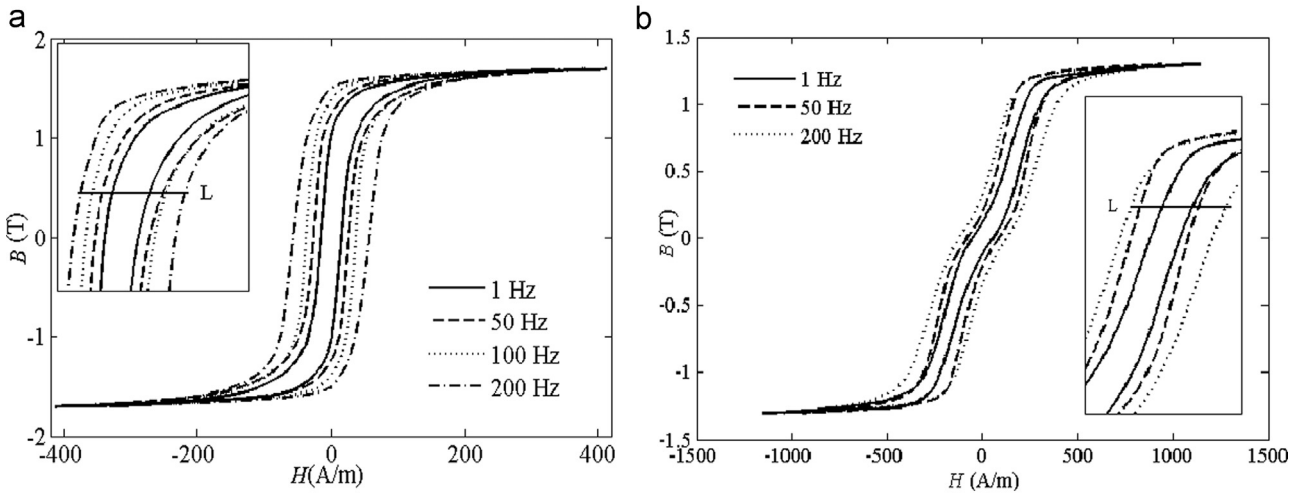

Fig. 1. Measured dynamic loops (Hi–B material, 27M-OH) (a) RD (b) TD.

Table 1
Core loss components in RD and TD.

Loss (J/m^3)	RD	TD
W_{hyst}	28.67	123.43
W_{class}	15.44	15.44
W_{exc}	17.43	155.31

Table 2
Static model parameters for RD and TD.

Parameters	RD	TD
M_s (A/m)	1.43×10^6	1.06×10^6
a (A/m)	68	80
k (A/m)	18	60
α	4.90×10^{-5}	4.90×10^{-5}
c	0.44	0.44
K_1(J/m^3)	3.10×10^2	7.20×10^2

3. Modeling of RD and TD static loops

GO laminations display strong anisotropic behaviour due to arrangement of their crystallites in the preferred RD orientation [3] which can be obtained according to the Goss orientation i.e., crystallites with their [001] easy axis close to RD and their (110) plane almost along the lamination surface.

The original JA description simulates the magnetic hysteresis using reversible and irreversible domain wall motions under the assumption of isotropic nature of materials [2]. Significant attempts have been made in the literature for inclusion of anisotropy and texture effects in the JA model [27–29]. A modified JA model, which is able to predict narrow-waist RD loops and complex-shaped TD loops, has been proposed recently in [11]. The model assumes that GO Fe–Si materials maintain as a whole cubic symmetry with axes of individual crystals along the global cubic axes [30]. The crystalline structure and texture of GO materials is included in the model by an appropriate energy term which depends on the angle between the magnetization direction and RD, and it gives the highest energy level at 55° (approximately) from RD. The anhysteretic magnetization has been modified by introducing an additional (anisotropic) energy term. The anhysteretic magnetization (M_{an}) can be expressed as a function of the magnetized direction [27]

$$M_{an} = M_s \frac{\int_0^{\pi} \exp(E/k_BT) \sin\theta \cos\theta \, d\theta}{\int_0^{\pi} \exp(E/k_BT) \sin\theta \, d\theta} \tag{3}$$

where M_s is the saturation magnetization, k_BT is the thermal energy of the system, and θ is the angle between the applied field and the direction of magnetic moments [11]. In the presence of anisotropy, the energy equation becomes,

$$E = -\mu_0 M_s (H + \alpha M) + E_{an} \tag{4}$$

where M and H are the total magnetization and the applied magnetic field, respectively, whereas μ_0 is the magnetic permeability of free space. The magneto-crystalline anisotropy energy (E_{an}) of a single cubic crystal can be expressed [1] as

$$E_{an} = K_0 + K_1\left(\alpha_1^2\alpha_2^2 + \alpha_2^2\alpha_3^2 + \alpha_3^2\alpha_1^2\right) + K_2\alpha_1^2\alpha_2^2\alpha_3^2 \tag{5}$$

where α_1, α_2, and α_3 are the direction cosines of the magnetization vector with respect to the three crystal axes. K_0, K_1, and K_2 are anisotropy constants. Only the second term of Eq. (5) is taken into consideration for anisotropy energy description which gives reasonably accurate results [11]. The direction cosines of the magnetization vector can be expressed in polar coordinates ($\alpha_1 = \left(1/\sqrt{2}\right)\sin\varphi$, $\alpha_2 = \left(1/\sqrt{2}\right)\sin\varphi$, and $\alpha_3 = \cos\varphi$; where, φ is the angle between the magnetization direction and RD) as given in [31].

The modification of the original description may be attributed a physical interpretation. The extended Eq. (4) considers the contributions from 180° and 90° domain walls to the magnetization process. The hysteretic behavior can be achieved by using an offset from the "anhysteretic" magnetization associated with Eq. (3). The offset represents the irreversible domain wall motion with pinning effects. The resulting differential susceptibility can be expressed as [2]

$$\frac{dM}{dH} = \frac{M_{an}(H) - M_{irr}(H)}{(k\delta/\mu_0) - \alpha(M_{an}(H) - M_{irr}(H))} + c\left(\frac{dM_{an}}{dH} - \frac{dM}{dH}\right) \tag{6}$$

where, δ is a directional parameter with the value of $+1$ for $dH/dt > 0$ and -1 for $dH/dt < 0$, whereas M_{irr} is the irreversible magnetization. The model can also be expressed in its inverse form which is particularly useful in numerical implementation and typical measurement systems [21] as

$$\frac{dM}{dB} = \left[\frac{\left(\frac{c}{\mu_0}\frac{dM_{an}}{dH_e}\right) + \left((1-c)\frac{dM_{irr}}{dB_e}\right)}{1 + \left((1-\alpha)c\frac{dM_{an}}{dH_e}\right) + \left(\mu_0(1-\alpha)(1-c)\frac{dM_{an}}{dH_e}\right)}\right]. \tag{7}$$

The modified model has six parameters (M_s, a, k, c, α, K_1). As pointed out in [11], a physical interpretation may be attributed to them. A hybrid optimization technique described in [32] is used for determining the model parameters from the measured quasi-static major loops for both directions. These optimized parameter values are given in Table 2.

The computed hysteresis loops with the obtained parameters are in close agreement with the measured curves as evident from Fig. 2. Maximum values of mean squared error do not exceed 5% (the highest error is obtained at knee region on the TD loop) for loops in the two principal directions.

4. Modeling of dynamic loops

The total energy losses can be represented as the sum of the static hysteresis loss, the classical loss, and the excess loss using a thin sheet model (TSM) [13]. The static hysteresis losses are the measured losses in a DC condition or at a very low frequency. The loss component has different values in different directions as can be observed in Table 1. The classical loss depends on the thickness and resistivity of the material and hence this loss will remain the same for all directions [3]. Therefore the parameter k_e remains the same for RD and TD and is calculated directly using Eq. (2). The field associated with classical eddy currents can be rewritten from this equation as

$$H_{class} = k_e\left(\frac{dB}{dt}\right)^2 \tag{8}$$

On the other hand, the excess losses are calculated by subtracting the sum of the static hysteresis and classical eddy losses from the total losses. This component of the dynamic loss changes with respect to direction as discussed in the previous section. The excess losses can be represented using the magnetic viscosity approach as [33]

$$W_{excess} = \oint_{cycle}\left[\frac{1}{r(B)}\frac{dB}{dt}\right]^{1/v}\frac{dB}{dt}\,dt \tag{9}$$

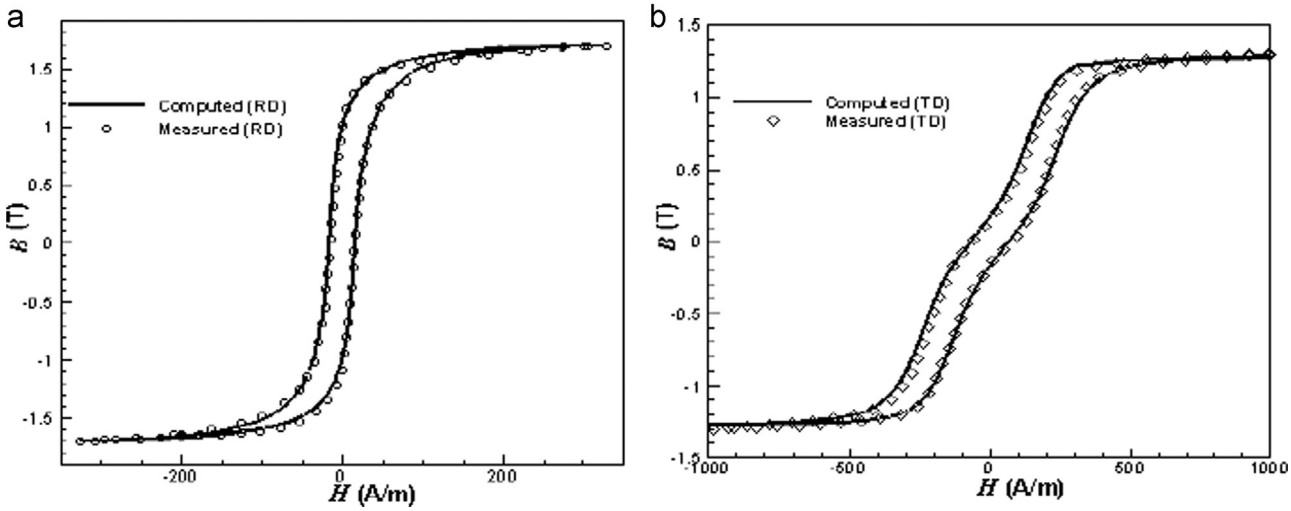

Fig. 2. Measured and computed static major loops of RD and TD.

where v is a parameter which controls the model dynamics and the function $r(B)$ is known as dynamic magnetic resistivity. The corresponding excess field strength is given as

$$H_{exc} = \left| \frac{1}{r(B)} \frac{dB}{dt} \right|^{1/v} \tag{10}$$

The function $r(B)$ may be written in the form [20]

$$r(B) = R_m \left(1 - \frac{B^2}{B_m^2} \right) \tag{11}$$

The function can control loop shapes and the exponent v can be used to predict the arbitrary frequency dependence of the excess losses [20]. In order to avoid possible singularity in Eq. (8) [21], the B_m term in the denominator of Eq. (10) has been multiplied by 1.01, yielding

$$r(B) = R_m \left(1 - \frac{B^2}{(1.01 \times B_m)^2} \right) \tag{12}$$

The viscosity-based approach offers flexibility in terms of two adjustable parameters (the value of exponent v and the form of function $r(B)$). In the present paper the approach which assumes a fixed value of exponent $v=2$ (which corresponds to Bertotti's $f^{1/2}$dependence for the excess loss) is considered. On the other hand, the value of R_m coefficient in the function $r(B)$ is adjusted in different parts of the loop in order to match the modeled and measured curves [33]. Different values of the coefficient in different induction intervals may have their source in varying contributions of different phenomena affecting the physics of magnetization process (as shown in Fig. 3) and their interaction with eddy currents generated in the conductive material.

The procedure for calculating dynamic hysteresis loops using the field separation approach combined with the static modified JA model is given in Fig. 4.

5. Results and discussions

The following relationships have been used in calculations of dynamic hysteresis loops depicted in Figs. 5 and 6. For RD, excitation frequencies are in the range of 50–200 Hz and the maximum flux density value is set to 1.7 T.

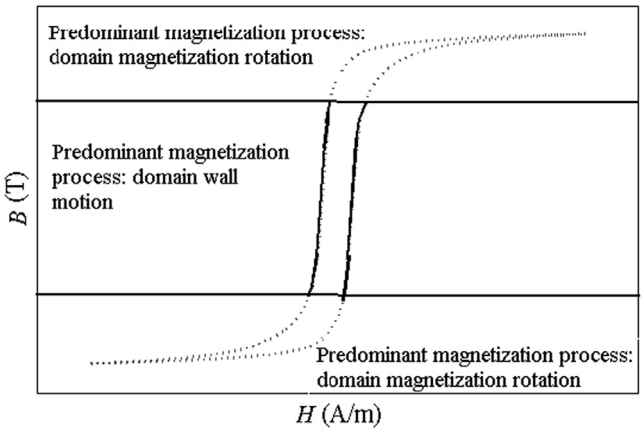

Fig. 3. Different mechanisms of magnetization process along the hysteresis loop.

$$r(B_\delta) = \begin{cases} 0.2807\left(1 - \left(\frac{B}{1.01B_m}\right)^2\right); & \text{if } B_\delta < 0 \text{ T} \\ 0.2846\left(1 - \left(\frac{B}{1.01B_m}\right)^2\right); & \text{if } B_\delta \in \langle 0 \text{ T}; 1 \text{ T} \\ 0.5614\left(1 - \left(\frac{B}{1.01B_m}\right)^2\right); & \text{if } B_\delta \geq 1 \text{ T} \end{cases}$$

For TD at maximum flux density value of 1.3 T.
case a) excitation frequencies: 50 and 100 Hz

$$r(B_\delta) = \begin{cases} 0.5297\left(1 - \left(\frac{B}{1.01B_m}\right)^2\right); & \text{if } B_\delta < -1 \text{ T} \\ 1.6499\left(1 - \left(\frac{B}{1.01B_m}\right)^2\right); & \text{if } B_\delta \in \langle -1 \text{ T}; 0 \text{ T} \\ 0.7945\left(1 - \left(\frac{B}{1.01B_m}\right)^2\right); & \text{if } B_\delta \geq 0 \text{ T} \end{cases}$$

case b) excitation frequencies: 150 and 200 Hz

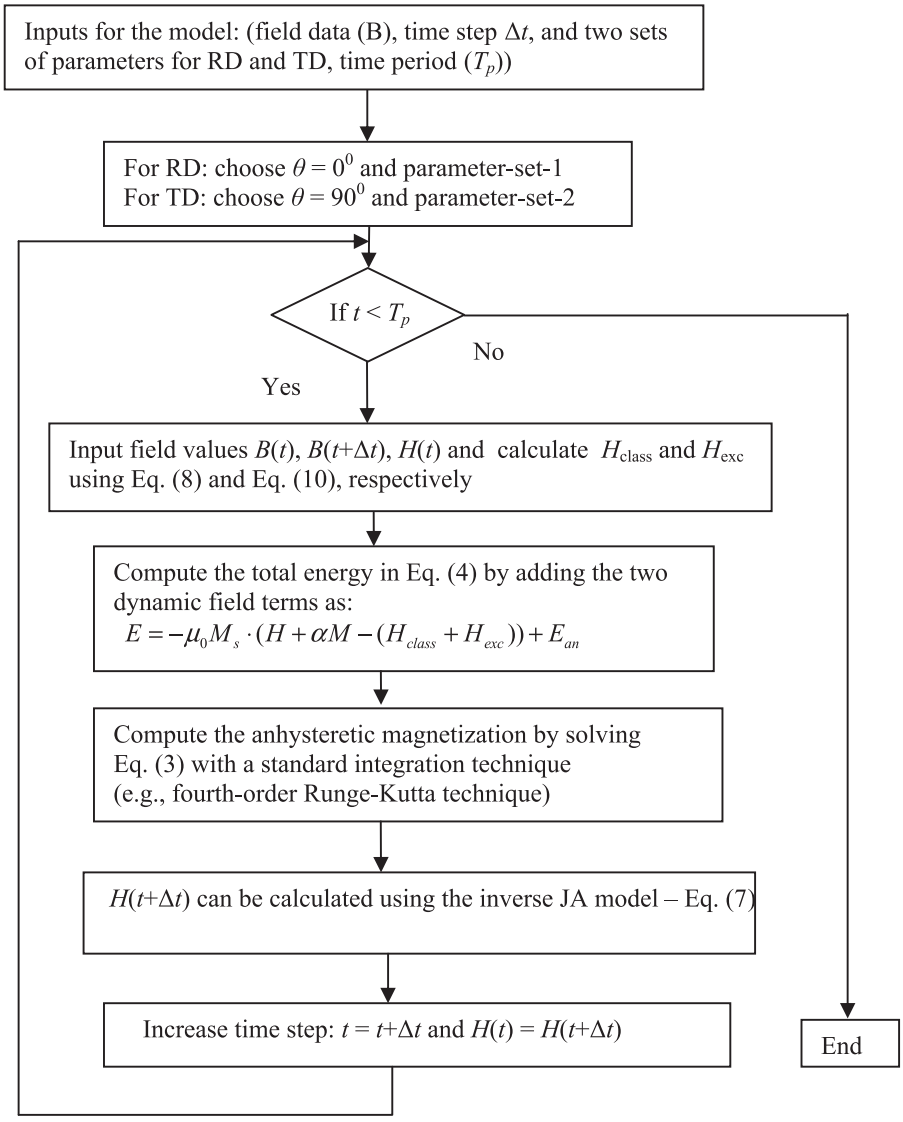

Fig. 4. Chart illustrating the computation of dynamic loops.

$$r(B_\delta) = \begin{cases} 0.5297\left(1 - \left(\frac{B}{1.01Bm}\right)^2\right); & \text{if } B_\delta < -1\ \text{T} \\ 1.2908\left(1 - \left(\frac{B}{1.01Bm}\right)^2\right); & \text{if } B_\delta \in \langle -1\ \text{T};\ 0\ \text{T}) \\ 0.7945\left(1 - \left(\frac{B}{1.01Bm}\right)^2\right); & \text{if } B_\delta \geq 0\ \text{T} \end{cases}$$

where B_δ denotes the product $B\delta$; $\delta = \pm 1$ is the sign of the derivative dB/dt[33].

The results of modelling are presented in Figs. 5 and 6 for RD and TD, respectively. It should be noticed that for RD, a single definition for function $r(B_\delta)$ suffices for the description in a wide range of excitation frequencies. The maximum mean squared error between the measured and the modeled loops is 5.2%. This discrepancy is obtained for $f = 100$ Hz (case depicted in Fig. 5b).

For the TD loops, it was found that better modelling results could be obtained using two separate definition sets of $r(B_\delta)$ for lower ($f \in \langle 50;\ 100\rangle$ Hz) and higher ($f \in \langle 150;\ 200\rangle$ Hz) excitation frequencies. However the different $r(B_\delta)$ values are evident only in the intermediate induction range $B_\delta \in \langle -1\ \text{T};\ 0\ \text{T}\rangle$. The difference may be attributed to the complicated mutual interactions between 180° and 90° domain walls and eddy currents in that induction range. In this direction, the domain wall process is accomplished by rearrangement of domain walls into 90° and 180° domain walls, which leads to variations in domain wall spacings [3,26,34]. According to some researcher [34], the suggested dependency on frequency of the from $f^{1/2}$ may also be related to the rearrangement of domain structure.

The maximum mean squared error between the measured and the modelled loops does not exceed 6.5%; this value is obtained for $f = 50$ Hz (the case shown in Fig. 6a)).

6. Conclusions

This paper presents a comprehensive approach for accurate description of dynamic loops in RD and TD of GO laminations. It also discusses a loss separation scheme using a three-component approach in the two principal directions. The hysteresis and excess components of the core losses vary with the direction of the applied field. The variation in static hysteresis losses is qualitatively explained in terms of changes in the domain configuration for RD/TD directions and it results from different roles played by the 180° and 90° domain walls during the magnetization process. This leads to highly steep and narrow waist RD loops and complex shaped TD

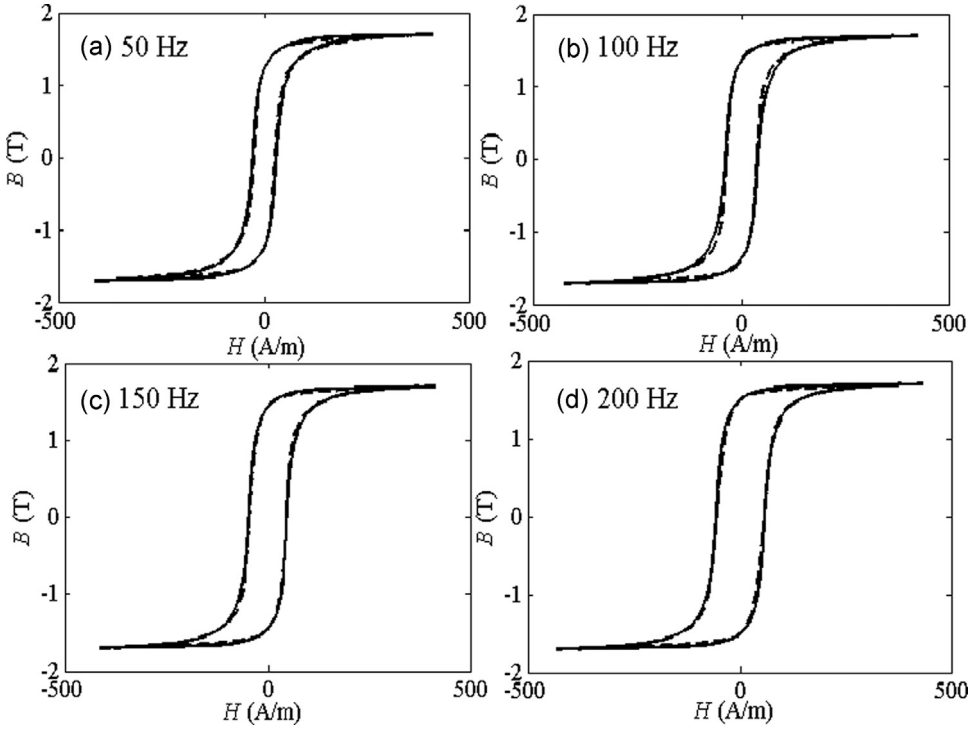

Fig. 5. Computed and measured dynamic loops in RD (dashed line – measurements, solid line – modelling).

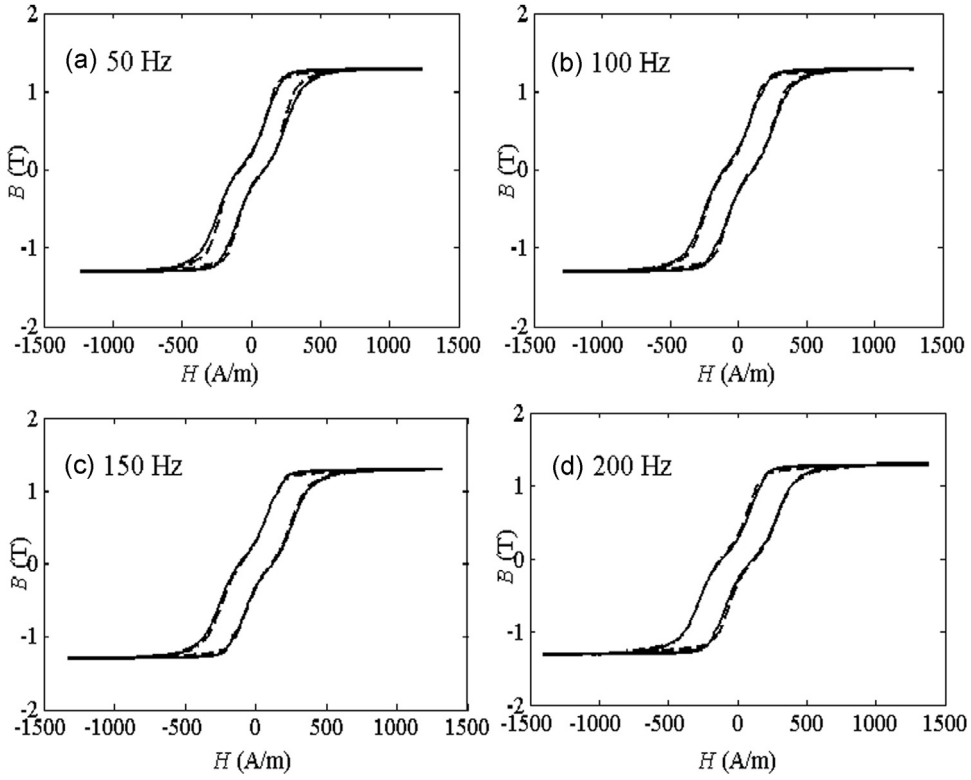

Fig. 6. Computed and measured dynamic loops in RD (dashed line – measurements, solid line – modelling).

loops. A modified JA model is used to describe static hysteresis loops in RD and TD. The modification is aimed to take into account the contributions of both kinds of domain walls in the definition of the "anhysteretic" function which is the backbone of the description.

In order to take into account the complex shapes of dynamic hysteresis loops the magnetic viscosity approach has been adopted to describe the excess loss component in the three-term loss separation scheme. This approach may precisely characterize the arbitrary loss–frequency relationship and anomalous shapes of

dynamic loops in RD and TD. The exponent v is used to control the arbitrary loss–frequency behavior whereas the anomalies in loop shapes can be handled by a modification of the function $r(B)$. The function is adjusted along the loop in order to predict correct loop shapes for both directions.

The proposed description has been validated using measured curves obtained under dynamic magnetization conditions with excitation frequencies in the range: $f \in \langle 50; 200 \rangle$ Hz. The model may be useful for the designers of magnetic circuits in electric machines. Its combination with a vector hysteresis model can make it possible to carry out a numerical analysis of core-joints and corner-regions in transformers. The issue shall be the subject of forthcoming research.

References

[1] G. Bertotti, Hysteresis in Magnetism, Academic, San Diego, CA, 1998.
[2] D.C. Jiles, D.L. Atherton, J. Magn. Magn. Mater. 61 (1986) 48–60.
[3] S. Shin, R. Schaefer, B.C. DeCooman, J. Appl. Phys. 109 (2011) 07A3071.
[4] J.E.L. Bishop, J. Magn. Magn. Mater. 49 (1984) 241–249.
[5] G.F. Mechler, R.S. Girgis, IEEE Trans. Power Deliv. 13 (1998) 532–537.
[6] E. Hajipour, P. Rezaei, M. Vakilian, M. Ghafouri, J. Electromagn. Anal. Appl. 3 (2011) 430–438.
[7] H. Yoon, C.S. Koh, Int. J. Comput. Math. Electr. Electron. Eng. 33 (2014) 14–27.
[8] A. Moses, J. Mater. Eng. Perform. 1 (1992) 235–239.
[9] A. Nourdine, A. Kedous-Lebouc, G. Meunier, T. Chevalier, IEEE Trans. Magn. 36 (2000) 1230–1233.
[10] A. Nourdine, A. Kedous-Lebouc, G. Meunier, T. Chevalier, IEEE Trans. Magn. 37 (2001) 3340–3344.
[11] A.P.S. Baghel, S.V. Kulkarni, J. Appl. Phys. 113 (2013) 043908.
[12] F. Fiorillo, L.R. Dupre, C. Appino, A.M. Rietto, IEEE Trans. Magn. 38 (2002) 1467–1476.
[13] N. Sadowski, N.J. Betistela, J.P.A. Bastos, L.M. Mazenc, IEEE Trans. Magn. 38 (2002) 797–800.
[14] D.C. Jiles, J. Appl. Phys. 76 (1994) 5849–5855.
[15] K. Chwastek, Math. Comput. Model. Dyn. Syst. 15 (2009) 95–105.
[16] H. Li, Q. Li, X. Xu, T. Lu, J. Zhang, L. Li, IEEE Trans. Magn. 47 (2011) 1094–1097.
[17] A.P.S. Baghel, S.V. Kulkarni, IEEE Trans. Magn. 50 (2014) 369–372.
[18] S.E. Zirka, Y.I. Moroz, R.G. Harrison, K. Chwastek, J. Appl. Phys. (2012) 043916-1–043916-7.
[19] S.E. Zirka, Y.I. Moroz, P. Marketos, A.J. Moses, D.C. Jiles, T. Matsuo, IEEE Trans. Magn. 44 (2008) 2113–2126.
[20] S.E. Zirka, Y.I. Moroz, P. Marketos, A.J. Moses, Physica B 343 (2004) 90–95.
[21] A.P.S. Baghel, S.K. Shekhawat, S.V. Kulkarni, I. Samajdar, Physica B 448 (2014) 249–353.
[22] K. Chwastek, Philos. Mag. Lett. 90 (2010) 809–817.
[23] S.E. Zirka, Y.I. Moroz, P. Marketos, A.J. Moses, IEEE Trans. Magn. 41 (2005) 1109–1111.
[24] J.W. Shilling, W.G. Morris, M.L. Osborn, P. Rao, IEEE Trans. Magn. 14 (1978) 104–109.
[25] M.F. de Campos, in: Proceedings of XVIII IMEKO World Congress, Rio de Janeiro, Brazil, 2006.
[26] G.W. Wiener, K. Foster, D.S. Shull, J. Appl. Phys. 38 (1967) 1102–1103.
[27] A. Ramesh, D.C. Jiles, J.M. Roderick, IEEE Trans. Magn. 32 (1996) 4234–4236.
[28] A. Ramesh, D.C. Jiles, Y. Bi, J. Appl. Phys. 81 (1967) 5585–5587.
[29] D.C. Jiles, A. Ramesh, Y. Shi, X. Fang, IEEE Trans. Magn. 33 (1997) 3961–3963.
[30] M. Celasko, P. Mazzetti, IEEE Trans. Magn. 5 (1969) 372–378.
[31] G.H. Shirkoohi, M.A.M. Arikat, IEEE Trans. Magn. 30 (1994) 928–930.
[32] A.P.S. Baghel, S.V. Kulkarni, IET Electr. Power Appl. 6 (2012) 689–695.
[33] S.E. Zirka, Y.I. Moroz, P. Marketos, A.J. Moses, IEEE Trans. Magn. 42 (2006) 2121–2132.
[34] L.R. Dupre, F. Fiorillo, J. Melkebeek, A.M. Rietto, C. Appino, J. Magn. Magn. Mater. 215-216 (2000) 112–114.